Miniature forward-viewing spectrally encoded endoscopic probe

Adel Zeidan* and Dvir Yelin

Faculty of Biomedical Engineering, Technion—Israel Institute of Technology, Haifa 3200003, Israel
**Corresponding author: az@tx.technion.ac.il*

Received April 1, 2014; revised June 21, 2014; accepted June 21, 2014;
posted June 24, 2014 (Doc. ID 209214); published August 13, 2014

Spectrally encoded endoscopy is a promising technique for minimally invasive imaging, allowing high-quality imaging through small diameter probes that do not require rapid mechanical scanning. A novel optical configuration that employs broadband visible light and dual-channel imaging is used to demonstrate a miniature forward-viewing probe having a high number of resolvable points, low speckle contrast, negligible backreflections, and high signal-to-noise ratio. The system would be most suitable for imaging through narrow ducts and vessels for clinical diagnosis at hard-to-reach locations in the body. © 2014 Optical Society of America

OCIS codes: (170.2150) Endoscopic imaging; (110.2350) Fiber optics imaging.
http://dx.doi.org/10.1364/OL.39.004871

Using only a single-fiber and a miniature optical assembly, spectrally encoded endoscopy (SEE) [1] has been shown promising for minimally invasive imaging in hard-to-reach locations within the body. Unlike other single fiber endoscope technologies, including distal mirror scanning [2,3], resonant fiber scanning [4], and endoscopic optical coherent tomography [5,6], SEE probes do not require rapid distal scanning, allowing for flexible submillimeter-diameter probes that do not contain moving parts. Interferometric SEE has been shown capable of 3D [7], subsurface [8], and Doppler [9] imaging with a high number of resolvable points and high signal-to-noise ratios (SNRs). Dual-clad fibers have been shown useful for reducing speckle contrast, increasing depth of field, and improving image brightness [10]; however, these probes often suffer from significant cross talk between the light-guiding channels, which results in a high background noise. Recently, we showed that by using two separate fibers for the illumination and collection channels [11,12], interchannel cross talk could be eliminated without substantial increase to the overall probe diameter.

A SEE probe would be ideal for imaging within confined environments, such as narrow ducts; nevertheless, recent SEE probes were designed with large side-viewing angles [7,13] due to the large beam deflections caused by high groove-density gratings. For many applications that require navigation through narrow passages and ducts, for example, the lack of forward-viewing capability is a significant drawback, and in cases where external visual guidance is not available, current SEE probes simply cannot be used for such applications.

In this work, we design and construct a forward-viewing spectrally encoded endoscopic probe capable of high-speed imaging with a high number of resolvable points. Using low spatial coherence illumination and a wavelength-encoded imaging channel, speckle noise was significantly reduced and backreflections were insignificant. The forward-viewing SEE system is schematically illustrated in Fig. 1. The illumination channel was composed of a low-coherence supercontinuum laser-driven light source (EQ-99FC, Energetiq Technology, Inc.) coupled to a multimode fiber having a 200 μm diameter core (FG200LCC, Thorlabs, Inc.) that has been previously shown effective for reducing speckle noise [12]. The distal end of the illumination fiber was polished at a 40° angle, resulting in an off-axis elliptical illumination spot. Broadband light backscattered from the sample was deflected by a distal SF-66 glass prism toward a transmission diffraction grating (1379 lines/mm), deflected again toward the main optical axis by another identical prism, and coupled into a single-mode fiber (S460HP, Thorlabs, Inc.) using a gradient-index lens.

The 1 mm diameter probe optics (Fig. 1, inset) were assembled from homemade components that were cut and polished down to the desired dimensions. The 1 mm diameter SF-66 prisms were laser cut from a larger glass slab tilted by 18.1° with respect to the beam axis, and the silica spacer was prepared by cleaving and polishing a 1 mm core diameter multimode fiber (FT1000UMT, Thorlabs, Inc.). The grating cutting procedure was described in detail in a previous publication

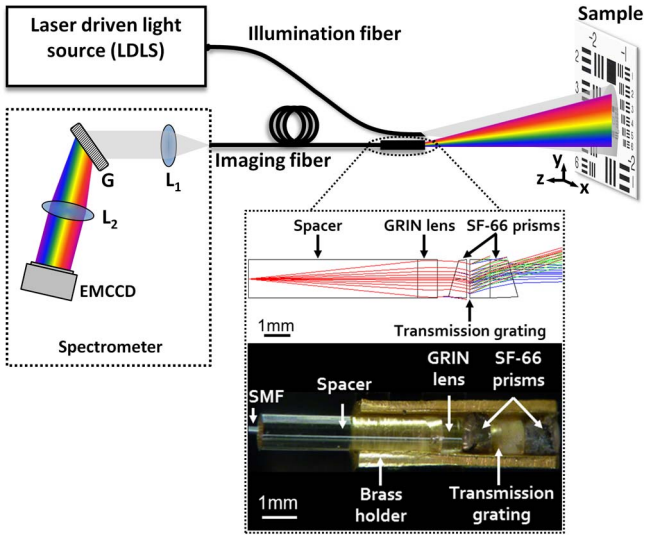

Fig. 1. Forward-viewing SEE system. L1, L2, achromatic lenses; G, transmission grating; EMCCD, electron-multiplying charge-coupled device. Inset: schematic drawing and a photograph of the probe. SMF, single-mode fiber; GRIN, gradient index.

[12]. The probe was assembled by aligning and gluing its components inside a hollow brass semi-cylinder using UV-curing optical adhesive.

Light emanating from the proximal fiber end was analyzed using a homebuilt spectrometer that is composed of an achromatic lens for beam collimation, a 1379 lines/mm transmission grating, and a 50 mm focal length lens that focuses the different spectral components onto a high-sensitivity electron-multiplication CCD array (200×1600 pixels, DU970N-BV, Andor Technology). The optical parameters of the prism-grating-prism assembly at the distal end of the probe were chosen so that the shortest wavelength would emanate parallel to the main optical axis of the probe, while an angle of approximately 27° is formed between the longest wavelength and the optical axis. A 2D image could be formed through probe rotation about the main optical axis, resulting in a circular field of view where the longest wavelength scans the circumference of the image circle and the shortest wavelength is nearly static at the center of the field of view.

In order to measure the optical performance of the system, a 1951 USAF scattering resolution target was mounted on a linear translation stage at the focal plane of the probe, approximately 7 mm from its distal end (Fig. 1). As the sample was scanned in the x axis, the reflected spectra were continuously captured, normalized to a reference spectrum, and stitched together to form a 2D image (Fig. 2(a)). The linear field of view and the lateral resolution (edge response, FWHM) were 3.6 mm and 6.6 μm, respectively, resulting in approximately 550 resolvable points along a single spectrally encoded line. These numbers are in good agreement with the expected theoretical values of 3.9 mm and 5.9 μm for the field of view and the lateral resolution, respectively. A relatively low speckle contrast of 0.11 was evident in the image due to the finite spatial coherence of the light emanating from the large aperture of the illumination fiber [12]. The lateral resolution had dropped to one-half of its maximum value approximately 3 mm before and after the focal plane, corresponding to an effective depth of field of 6 mm. The softening at the top and bottom edges of the image was caused by various optical aberrations, mainly field curvature and coma, originated at both the probe and spectrometer optics. The visibility of these aberrations was enhanced by the normalization to a reference spectrum. The lateral field of view Y was approximately linearly dependent on the axial location of the sample according to $Y = z \tan \theta$, where z denotes the sample distance from the diffraction grating and θ denotes the angle between the propagation directions of the shortest and the longest wavelengths ($\theta = 27°$). These variations in the field of view (and the resulting magnifications) could be noted and quantified by comparing images of the resolution target placed before (Fig. 2(b)) and after (Fig. 2(c)) the focal plane.

Imaging a plane parallel to the optical axis of the probe (e.g., the wall of a narrow duct) was demonstrated by placing the resolution target with its plane parallel to the probe axis at different distances (Δy) from the probe axis (Fig. 3(a)). Despite the large angle (~77°) between the target normal and the direction of propagation of the center wavelength, the large 6 mm depth of field still allowed high-resolution imaging across a large central portion of the field of view (Fig. 3(b)). Also noted is a gradual shift in the field of view as a function of the target displacement.

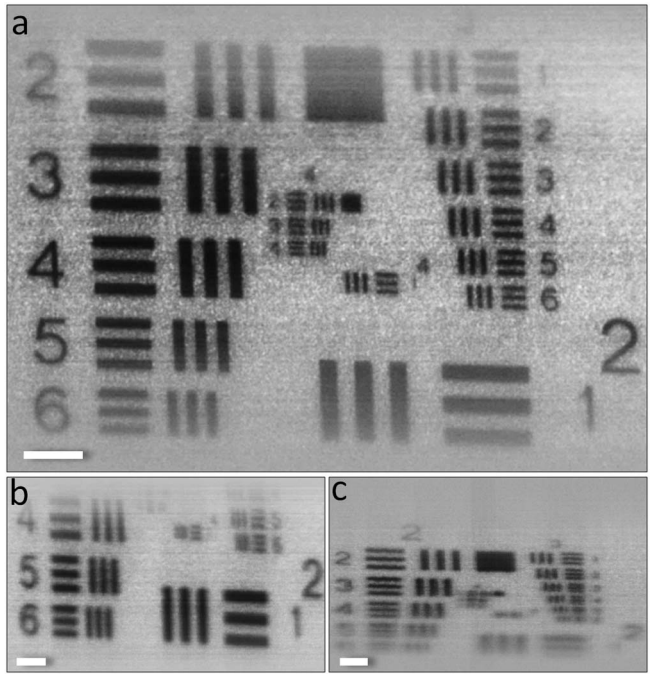

Fig. 2. (a) Image of a 1951 USAF scattering resolution target 7 mm from the distal end of the probe. (b) Same as Fig. 2(a), 4 mm from probe. (c) Same as Fig. 2(a), 10 mm from the probe. Scale bars, 440 μm.

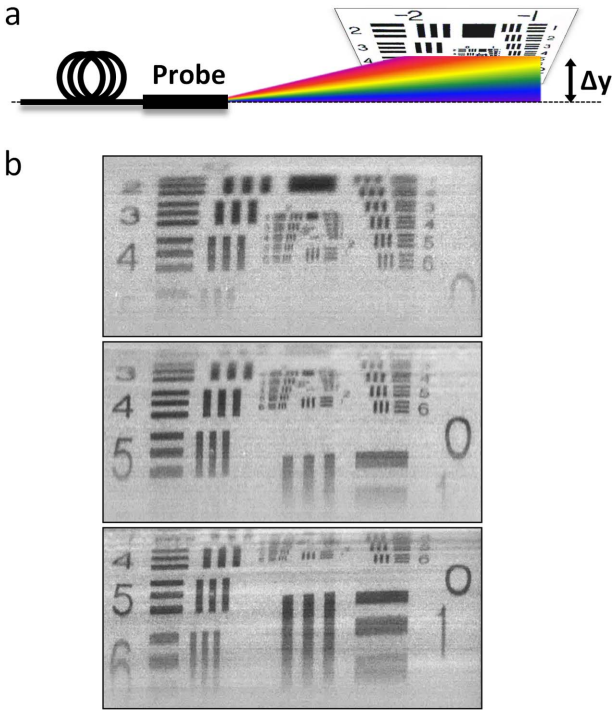

Fig. 3. Imaging a resolution target parallel to the probe axis. (a) Schematic illustration of the imaging configuration. (b) Imaging at different radial displacements from the optical axis. Δy, from top to bottom: 2 mm, 1.6 mm, 1.2 mm.

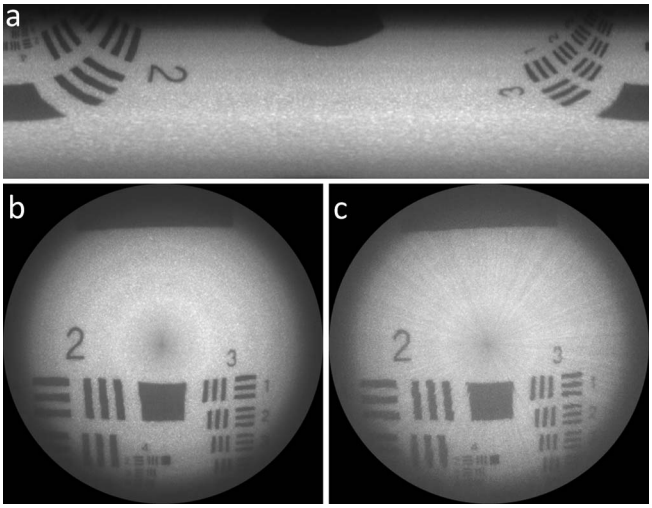

Fig. 4. (a) 2D raw image acquired during a full rotation of the resolution target. Exposure time was 10 ms per line. (b) Polar coordinates presentation of Fig. 4(a). (c) The same as Fig. 4(b) using exposure time of 10 μs per line.

In order to simulate image acquisition during probe rotation, the scattering resolution target was mounted perpendicular to the probe axis on a rotational platform (HR-3, Newmark Systems, Inc.) approximately 7 mm from the distal end of the probe. The 2D raw image composed of the sequentially acquired spectrally encoded lines following a full 360° rotation (Fig. 4(a)) was transformed to polar coordinates to obtain the actual circular field of view (Fig. 4(b)). The total angle of view of the probe was approximately 54°, resulting in an approximately 7 mm diameter image circle. Number of resolvable points in each image was approximately 1.1×10^6, estimated by dividing the total image area by the average area of a single resolution element. Exposure duration for each spectrally encoded line was 10 ms. At an exposure duration of 10 μs per line (limited by the camera electronics), image noise (Fig. 4(c)) was still acceptable (SNR = 14 dB), demonstrating the potential of the forward-viewing probe to image at up to 25 full circular frames per second. Some motion artifacts are visible in the image (Fig. 4(c)), caused probably by vibrations induced by the rotational scanning.

Previous demonstrations of SEE required interferometry to achieve high SNRs [7,14]. Here, high-speed imaging was achieved by means of a high brightness light source, a multimode illumination fiber, and a fast high-sensitivity camera. Signal efficiency could be further improved by increasing the overlap between the illumination spot and the spectrally encoded imaging line; for example, by using a more sophisticated optics at the distal end of the illumination fiber or by using several multimode fibers at the circumference of the probe. Obviously, these capabilities must be complemented by a reliable rotational scanning mechanism. Such mechanism had been demonstrated for SEE for a total rotation angle of 20° [7] and for spectrally encoded confocal microscopy for a full probe rotation [15,16]. For our miniature forward-viewing dual-channel probe, a new rotation mechanism needs to be developed that would provide up to 25 full revolutions per second through a rotary junction that maintains effective light coupling to both the illumination and imaging channels. Such couplers—for example, the RJ2 series rotary joints from Princetel, Inc.—are commercially available and could be adapted for this application. Finally, in comparison to a conventional side-viewing SEE probe, images from the forward-viewing probe would cover a continuous circular field of view with somewhat less resolvable points due to the oversampling near the optical axis, as well as minor clipping of the beam at the grating aperture (see Fig. 1). Otherwise, the image resolution, contrast, speed, and speckle would not be significantly different from those of a side-viewing probe equipped with similar grating and lens parameters.

In summary, a dual-channel SEE system with a forward-viewing 1 mm diameter probe was presented, which could provide clinicians with high image quality using a robust optical design that addresses some of the previous challenges of SEE. The system uses broadband visible light and multichannel imaging to provide 1.1×10^6 resolvable points at low 0.11 speckle contrast, short 10 μs line-exposure duration, large depth of field, and low backreflections. The use of visible light would allow future color imaging capabilities [11,13] and effective spectral imaging [17] for enhancing the potential for clinical diagnostics. The system would be useful for navigating through narrow vessels and ducts for imaging and diagnosis within hard-to-reach locations in the body.

The study was funded in part by the European Research Council starting grant (239986), Israel Science Foundation grant (716/09), and by the Adelis Foundation for brain research. This work was also supported in part by the Lorry I. Lokey Interdisciplinary Center for Life Sciences and Engineering.

References

1. G. J. Tearney, M. Shishkov, and B. E. Bouma, Opt. Lett. **27**, 412 (2002).
2. A. L. Polglase, W. J. McLaren, S. A. Skinner, R. Kiesslich, M. F. Neurath, and P. M. Delaney, Gastrointest. Endosc. **62**, 686 (2005).
3. C. Changho, K. Isamoto, and H. Toshiyoshi, IEEE Photon. Technol. Lett. **18**, 133 (2006).
4. E. J. Seibel and Q. Y. J. Smithwick, Lasers Surg. Med. **30**, 177 (2002).
5. G. J. Tearney, M. E. Brezinski, B. E. Bouma, S. A. Boppart, C. Pitris, J. F. Southern, and J. G. Fujimoto, Science **276**, 2037 (1997).
6. D. Wang, L. Fu, X. Wang, Z. Gong, S. Samuelson, C. Duan, H. Jia, J. S. Ma, and H. Xie, J. Biomed. Opt. **18**, 086005 (2013).
7. D. Yelin, I. Rizvi, W. M. White, J. T. Motz, T. Hasan, B. E. Bouma, and G. J. Tearney, Nature **443**, 765 (2006).
8. D. Yelin, B. E. Bouma, and G. J. Tearney, Opt. Express **16**, 1748 (2008).
9. D. Yelin, B. E. Bouma, J. J. Rosowsky, and G. J. Tearney, Opt. Express **16**, 14836 (2008).
10. D. Yelin, B. E. Bouma, S. H. Yun, and G. J. Tearney, Opt. Lett. **29**, 2408 (2004).
11. A. Abramov, L. Minai, and D. Yelin, Opt. Express **18**, 14745 (2010).
12. G. Engel, H. Genish, M. Rosenbluh, and D. Yelin, Biomed. Opt. Express **3**, 1855 (2012).

13. D. Kang, D. Yelin, B. E. Bouma, and G. J. Tearney, Opt. Express **17**, 15239 (2009).
14. D. Yelin, W. M. White, J. T. Motz, S. H. Yun, B. E. Bouma, and G. J. Tearney, Opt. Express **15**, 2432 (2007).
15. D. Kang, M. J. Suter, C. Boudoux, H. Yoo, P. S. Yachimski, W. P. Puricelli, N. S. Nishioka, M. Mino-Kenudson, G. Y. Lauwers, B. E. Bouma, and G. J. Tearney, Gastrointest. Endosc. **71**, 35 (2010).
16. D. Yelin, C. Boudoux, B. E. Bounia, and G. J. Tearney, Opt. Lett. **32**, 1102 (2007).
17. A. Abramov, L. Minai, and D. Yelin, Opt. Express **19**, 6913 (2011).